Environmental Geology (1996) 27: 1–15

H. Kucha · A. Martens · R. Ottenburgs · W. De Vos · W. Viaene

Primary minerals of Zn-Pb mining and metallurgical dumps and their environmental behavior at Plombières, Belgium

Received: 11 February 1995 / Accepted: 27 June 1995

Abstract The primary phases and minerals of the Plombières dumps include typical smelting furnace products such as metallic Fe, Pb, Cu, Zn, Fe–Zn alloys, carbides, phosphides, sulfides of Fe, Zn, Pb, Cu, Mn (alabandite), and FeAs. Spinels, mainly of Fe and Al, are common constituents of the primary assemblage; substitution by Zn, V, Cr, Ti, Mg, and Ca occurs. Primary phases also include the most common Zn-rich fayalite, Zn-rich Ca–Fe silicates, melilite, corundum, and apatite. Most of the Zn is incorporated in iron silicates, ZnO and ZnS. Lead occurs mainly as PbS, metallic lead, and is also present in coal residues. Cadmium is found mainly in metallic zinc and its alloys and in ZnO. The dumps also contain mining wastes composed of pyrite, melnikovite, and iron oxides produced by natural weathering of Zn–Pb ores. Melnikovite and iron oxides are rich in As, Pb, and Zn and possess an increased content of Tl. Leaching tests carried out on the surfaces of polished sections indicate that acid rain (solutions I and II) will mobilize mainly Zn and Cd and, to a much smaller extent, Pb and Sb. Leaching of metals by sulfate-chloride fluids present in the pore network of dumps (solutions III, IV, and V) depends on the pH, which in the dumps is controlled by the proportion of carbonates to sulfides. The more acid fluids leach both sulfides and silicates.

Introduction

Extensive Zn–Pb mining and smelting was carried out in the area of La Calamine and Plombières (Fig. 1) from the Middle Ages until the beginning of the present century, with a total production estimated at 1,100,000 t of metallic zinc and 130,000 t of metallic lead (Dejonghe and Jans 1983; Ladeuze and others 1991). This activity left huge tailings and smelting slag wastes (Fig. 2).

The Plombières dumps occupy an area of about 400 × 700 m with heaps of dumped material rising up to 20 m high. From their appearance, the dumps are generally composed of: (1) red to black iron oxides (about 55% of the dumped material) originating from weathering of both slags and mine waste, and often coated on the surface by a white gypsum cover (Fig. 3); (2) coal-rich black material (about 20%); (3) slag material (about 10%); (4) ash from power and heat generating plants (about 5%); (5) Zn–Pb mining waste (about 5%); (6) various rubble of bricks, ceramic pipes, and other dumped building materials (about 3%); and (7) clay containing variable amounts of fine-grained dolomite sand as a mineral dressing waste (about 2%).

According to the approximate waste volume, the total amount is probably 1.3 to 2 million tonnes. The dump area is drained directly by the small river Geul, which discharges into the Meuse. The overbank sediments of the Geul downstream of Plombières contain on average 480 ppm Pb, 2300 ppm Zn, 4.5 ppm Cd, and 16 ppm Cu (Leenaers 1989).

According to the mineral and chemical composition of the Zn–Pb ores (Dejonghe and Jans 1983) and the mineral dressing and smelting techniques (Dimanche and others 1979), the main minerals and smelting products residing in the Plombières dumps are: dolomite, calcite, clay minerals, goethite, quartz, sphalerite with 0.3–1.6 weight percent Cd, galena, pyrite, marcasite, smithsonite, cerussite, anglesite, willemite, barite, Zn–Fe spinels, chalcopyrite, bornite, and fluorite. The list of primary minerals mentioned in the Zn–Pb deposits also includes rare minerals of Ni, Co, Mn, and Hg (Dejonghe and Jans 1983), which may have supplied these metals to the slag material, to secondary weathering minerals, and to the groundwater.

During weathering of the dumps, part of the mineral load was dissolved and carried away in solution, while another part was reprecipitated as new secondary min-

H. Kucha (✉) · A. Martens · R. Ottenburgs · W. Viaene
Fysico-chemische Geologie, K.U. Leuven, Celestijnenlaan 200C, B-3001 Leuven, Belgium

W. De Vos
Geological Survey of Belgium, Jennerstraat 13, B-1040 Brussels, Belgium

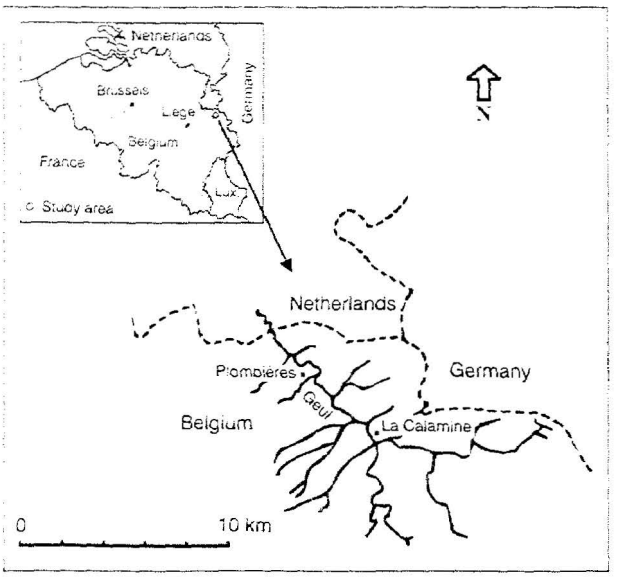

Fig. 1 Sketch showing the location of the main dumps in the tributary of the Geul river

Fig. 2 A general overview of the Plombières dumps. Elevated sections of the dump stay well above water level, but lower sections are often submerged

erals. These include (Van Tassel 1979): oxides of Zn, Fe, Cu; carbonates of Ca, Mg, Zn, Cu, Pb and Fe; sulfates of Fe, Pb, Cu, Cu–Al, Cu–Ca; and phosphates of Fe and Pb.

For the sake of simplicity, we divide the minerals identified in the dumps into two groups: primary, including all the mineral load from mine wastes, mineral dressing wastes, and blast furnace slags; and secondary minerals, which were formed in the dump environment. This paper treats only the primary phases/minerals. Inevitably some minerals, such as goethite, smithsonite, willemite, and anglesite, appear in both groups. These minerals are formed in the secondary environment of the dumps, but some of them already existed in the orebodies as natural weathering products and found their way to the dumps as mine waste and/or mineral dressing waste. For this group of minerals the distinction between primary and secondary origin can be made based on macro- and microtextures.

The aim of this paper is to present a systematic description of the primary mineral composition of dumps and the results of a number of leaching tests. An attempt will be made to quantify the mobility of heavy metals from dumps during weathering.

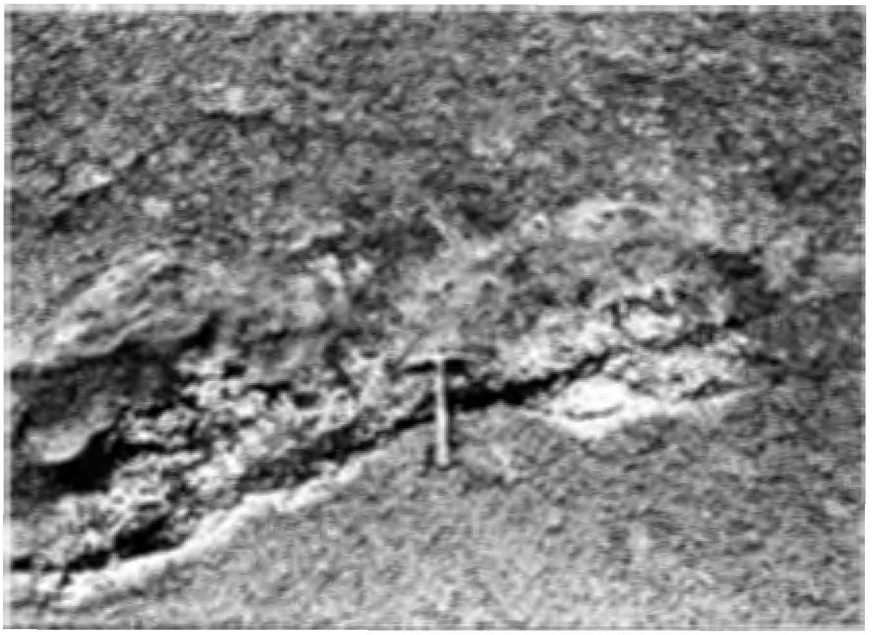

Fig. 3 Subvertical slope of metallurgical dump at Plombières covered in places by white goslarite and gypsum

Materials and methods

One hundred fifty samples were collected at the Plombières dumps, differentiated macroscopically according to color, luster, fabric, density, and abundance. These specimens are composed of iron oxides, coal, and graphite-rich fragments, slags, mine wastes, and silty clays. The weight of individual samples varies from 1 to a few kilograms.

For determination of the total concentration of elements, 1 g of the sample was decomposed in 4 ml concentrated HCl, 2 ml concentrated HNO_3, and 2 ml concentrated HF. After evaporation to half of the liquid volume, the procedure was repeated. After complete evaporation, the residue was dissolved in 20 ml 2.5N HCl. The extract was filtered and the fluid diluted to 50 ml with water. The Pb, Zn, Cu, Cd, Fe, Mn, K, and Ag concentrations in bulk samples were measured with an AAS Varian AA-1475. The insoluble residue (IR) was measured for each sample. Organic carbon was determined by ashing at 1000°C.

Representative samples were polished and analyzed by reflected light microscopy, which provided a base for further selection of specimens for microprobe study.

Microprobe analyses were made with a Camebax microprobe at the Université Catholique de Louvain, at 15 kV. Two sets of standards were used. The set for metals and sulfides included SKα and FeKα (FeS_2), MnKα, ZnKα (ZnS), CuKα, AsLα, CdLα, AgLα, SbLα, and PbMα (PbS). PKα was measured with an Fe_3P standard at 20 kV using a Jeol 733 probe at the Department of Material Sciences of the Katholieke Universiteit Leuven. The second set of standards included those for the analysis of aluminum silicates and consisted of oligoclase, leucite, fayalite, forsterite, wollastonite, rhodonite, sapphirine, rutile, chromite, and hematite.

SEM analyses were made with a Jeol JSM-6400 with a Link EXL-10/EDS system. XRD analyses were made with a Philips PW-1130 powder diffractometer and with a Gandolfi camera using Fe-filtered CoKα radiation.

Leaching tests were performed on the surfaces of some polished sections in order to assess the mobility of the heavy metals in the dump environment and to make a correct interpretation of the sequential leaching tests. The etching solutions were applied to polished surfaces as drops covering an area 4–5 mm in diameter. These tested areas were photographed prior to leaching to obtain reference pictures. Seven different solutions were applied to the polished surfaces. Solutions I and II were designed to mimic fresh rainwater during the initial stage of interaction with dump material. Solution I consisted of deionized water acidified to pH 5 by adding a small quantity of HNO_3. Solution II was similar except for its pH of 2, which increases the etching speed. Solutions III, IV, and V were designed to match the compositions of pore waters in the Plombières dumps. These fluids have a pH between 6.8 and 8.0. The three solutions have the same Cl^- and SO_4^{2-} contents (90 $\mu g\ l^{-1}$ and 825 $\mu g\ l^{-1}$, respectively), but they differ in their pH by addition of NaOH or HNO_3. Leaching solution III had a pH of 7.5, solution IV a pH of 5, and solution V a pH of 4. Solution VI contains sodium acetate and has pH 7 to test the solubility of the exchangeable cations, and solution VII again consists of sodium acetate acidified to pH 5 with HAc to determine soluble carbonates. The etching time varied between 0.5 min and 18 h.

Mineralogy and geochemistry of slags

The slags occur as fragments of centimeter to decimeter size often coated with gypsum (Fig. 3). The slag material studied is very heterogeneous, which makes it difficult to estimate the relative abundances of the mineral constituents. Thirty polished sections selected by examination of hand specimens were studied.

Silicate slag material makes up about 10% of the Plombières dump, but it is mineralogically the most complex material, so the mineralogical study was concentrated on it. It contains (weight percent): Fe 30.1–46.3, Mn 0.85–1.08, Zn 1.50–4.27, Pb 1.74–2.18, and (ppm): Cd 1.6–1.8 and Cu 555–1000. The main minerals of the slags are iron silicates such as fayalite, magnesium–fayalite, and ferroan melilite. Not only do they contain most of the iron in the slags, but also about half of the Zn. The other half of the Zn is present as sphalerite, wurtzite, and Zn spinels.

According to the analyses, the lead content of the slags is controlled by galena and metallic lead usually intergrown with pyrrhotite, bornite, and Fe–Ni arsenide. So in the primary slag material Pb, Cu, and As are usually positively correlated.

Phosphorus is mostly present in apatite and schreibersite (Fe_3P). Barium is present mainly in Ba-bearing melilite. The cadmium content in bulk slag material is relatively low (1.6–1.8 ppm). As will be described below, its content is controlled by metallic zinc and its alloys as well as by more abundant ZnO.

Metallic zinc and its alloys

Metallic zinc and its alloys Fe_1Zn_{11} and Fe_3Zn_{10} are common minor constituents of the slags studied. They are present as inclusions in the silicate matrix and in massive ZnO (Fig. 4). Metallic zinc forms grains up to 150 μm in size. It is often intergrown with Fe_1Zn_{11} and Fe_3Zn_{10}, which are known in the Zn–Fe binary system (Johansson and others 1968; Brandon and others 1974). Microprobe analysis (Table 1) shows that the studied metallic Zn, Fe_1Zn_{11}, and Fe_3Zn_{10} do not contain large amounts of other elements. Ni and Tl are the only admixtures found more frequently in zinc and its alloys, but their content does not exceed 0.31 weight percent (Table 1).

When freshly polished sections were immersed in solution I (pH 5), metallic zinc reacted rapidly and was converted into a hydroxide form within minutes, while the alloys remained essentially intact. The high reactivity of zinc compared to the chemical resistance of its alloys may

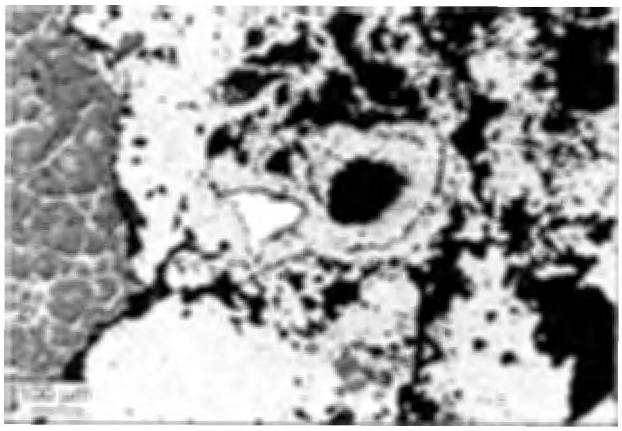

Fig. 4 Microphotograph of metallic zinc (white) and its Fe alloys embedded in massive ZnO (grey). Reflected light, sample 15/D, scale bar 100 μm

explain the frequent presence of small inclusions of Zn–Fe alloys in massive ZnO, whereas most metallic zinc has been transformed to massive ZnO.

Zinc oxide (ZnO, zincite)

Zinc oxide is a major component of the samples where metallic zinc and its alloys are found. It forms massive or porous accumulations up to 1 cm in size. ZnO has large unfilled cavities (Fig. 4), which appear black in reflected light. Smaller cavities may be lined by hydrozincite $Zn_5[(OH)_3\backslash CO_3]_2$ and then filled up with opaline silica. The ZnO studied contains traces of Mn, Fe, Ni, Cd, Tl, and Pb (Table 2). ZnO is slightly etched by solutions III and IV. The etching is more pronounced with solution V. This indicates that the solubility of ZnO in pore fluids of the dumps is strongly controlled by the pH.

Willemite [$Zn_2(SiO_4)$]

Willemite appears inside massive ZnO as subhedral crystals usually with sharp boundaries to the host zincite. In reflected light it appears considerably darker than Zn, due to its much lower refraction indices. The willemite studied contains significant amounts of (weight percent): Al 0.05–0.55, Ca 0.38–0.89, Fe 0.22–1.13, Mn 0.05–0.42, and Ba 0.07–0.43. During weathering it is replaced by hemimorphite or hydrozincite.

Sphalerite [(Zn,Fe)S] and wurtzite (Fe,Zn)S

Sphalerite appears to be one of the most common sulfide minerals in the studied samples (Fig. 5). It occurs intergrown with metallic lead (Fig. 6) but is often a member of complex sulfide–spinel intergrowths. Independent grains of ZnS are commonly intergrown with chalcopyrite. Sphalerite also occurs frequently in a ferroan melilite matrix together with Fe_2SiO_4 lamellae (Fig. 5), and wurtzite.

The sphalerite studied is Fe-rich (Table 3) but has low Mn and Cd contents. The copper content varies between 0.04 and 0.35 weight percent in homogeneous sphalerite.

Table 1 Microprobe composition of metallic zinc, lead, iron and its alloys (wt %)[a]

Mineral	Fe	Ni	Cu	Zn	Cd	Tl	Pb	As	Sb	*n*
Zn										
Min	≤0.03	≤0.03	≤0.03	99.54	≤0.05	≤0.07	≤0.09	≤0.05	≤0.04	4
Max	≤0.03	0.14	0.12	100.04	0.34	0.28	1.19	≤0.05	≤0.04	
Mean	≤0.03	0.09	0.07	90.79	0.14	0.13	0.37	≤0.05	≤0.04	
Pb										
Min	0.05	≤0.03	≤0.04	≤0.04	≤0.07	≤0.07	93.62	≤0.07	2.18	4
Max	0.36	≤0.03	0.15	0.06	≤0.07	≤0.07	96.11	0.19	4.29	
Mean	0.22	≤0.03	0.07	0.05	≤0.07	≤0.07	95.18	4.80	3.30	
Fe										
Min	98.99	≤0.03	0.31	0.09	≤0.03	≤0.07	≤0.04	0.89	0.13	3
Max	100.09	≤0.03	0.42	0.10	≤0.03	≤0.07	≤0.04	1.03	0.20	
Mean	99.54	≤0.03	0.37	0.10	≤0.03	≤0.07	≤0.04	0.96	0.17	
Zn–Fe alloy										
Min	6.90	≤0.03	≤0.03	79.12	≤0.05	≤0.07	≤0.09	≤0.05	≤0.04	5
Max	20.40	0.31	≤0.03	92.85	0.38	0.31	≤0.09	≤0.05	≤0.04	
Mean	12.27	0.17	≤0.03	87.08	0.19	0.12	≤0.09	≤0.05	≤0.04	

[a] Sought but not detected: S ≤ 0.06, Mn ≤ 0.03. *n*: number of microprobe analyses

Table 2 Microprobe composition of ZnO (wt %)

	S	Mn	Fe	Ni	Cu	Zn	Cd	Tl	Pb	*n*[a]
Min	≤0.04	≤0.02	≤0.03	≤0.02	≤0.02	76.11	0.05	≤0.06	≤0.08	6
Max	0.06	0.09	0.14	0.18	0.05	79.54	0.20	0.41	0.78	
Mean	0.05	0.06	0.10	0.09	0.03	77.84	0.16	0.20	0.50	

[a] *n*: number of microprobe analyses

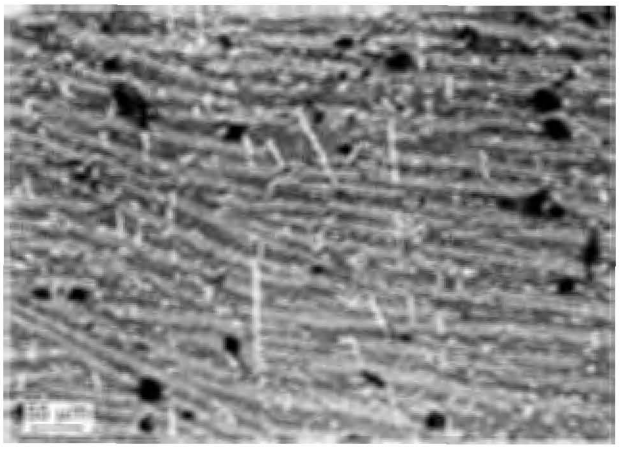

Fig. 5 Microphotograph of the silicate matrix composed of melilite (grey) and needles of Zn-bearing olivine (light grey) and of inclusions of sphalerite (small isometric inclusions) and wurtzite (long white needles). Reflected light, sample PL-D8, scale bar 55 μm

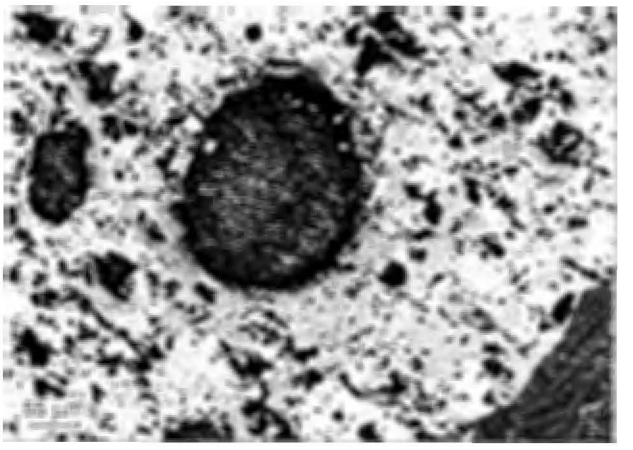

Fig. 6 Microphotograph of a complex intergrowth composed of metallic lead (oval grains with dark grey bad polish) containing small brighter inclusions of FeAs, marcasite (white), pyrrhotite (white somewhat darker than marcasite), and sphalerite (light grey). In the right lower corner needles of olivine in the melilite matrix are present. Reflected light, sample 23, scale bar 55 μm

However, some sphalerite grains contain lamellae enriched in Cu (up to 1.78 weight percent), a feature also found in many natural sphalerites (Ramdohr 1969). The Mn and Cd contents are not significant in the ZnS studied (Table 3). This sphalerite should not be regarded as a naturally occurring mineral. At the high temperature in the blast furnace, ZnS was equilibrated with other sulfides through the MSS (monosulfide solid solution), and most Mn may have been expelled from the ZnS structure to form α-MnS (alabandite) which is not isostructural with sphalerite (β-ZnS).

ZnS is inert to solution I applied to the polished surface over a test period of 18 h. The only reaction observed on the polished section occurs with solution II and is limited to rendering visible microscopic streaks of galena and pyrrhotite residing in the ZnS matrix. After applying solution II for 80 min, polishing scratches become visible. During further tests up to 18 h, etching alongside polishing scratches progresses very slowly. In general, ZnS is also resistant to solution II over the test period.

Sphalerite is etched by solutions III, IV, and V. Solu-

Table 3 Microprobe composition of primary sulphides of slags (wt %)

Mineral	Mn	Fe	Cu	Zn	Ag	Cd	Pb	As	Sb	n^a
Pyrrhotite										
Min	≤0.01	59.64	0.78	≤0.01	≤0.04	≤0.03	≤0.04	≤0.04	≤0.05	3
Max	0.20	61.52	1.09	0.14	≤0.04	≤0.03	4.56	0.14	0.35	
Mean	0.12	60.52	0.95	0.05	≤0.04	≤0.03	1.64	0.09	0.16	
Sphalerite										
Min	0.08	9.52	0.04	52.74	≤0.03	0.05	≤0.04	≤0.04	≤0.04	7
Max	0.33	13.40	1.78	58.95	≤0.03	0.08	0.15	≤0.04	≤0.04	
Mean	0.17	11.60	0.53	55.25	≤0.03	0.06	0.06	≤0.04	≤0.04	
Wurtzite										
Min	0.37	32.35	0.57	29.98	≤0.04	0.04	≤0.05	≤0.04	≤0.04	3
Max	0.53	33.00	1.07	31.36	0.06	0.13	≤0.05	≤0.04	≤0.04	
Mean	0.46	32.78	0.83	30.80	0.05	0.10	≤0.05	≤0.04	≤0.04	
Alabandite										
Min	1.17	5.44	0.22	29.81	≤0.04	≤0.03	≤0.05	≤0.04	≤0.04	4
Max	24.60	32.70	0.58	45.55	≤0.04	0.13	≤0.05	≤0.04	≤0.04	
Mean	12.91	15.46	0.40	37.00	≤0.04	0.07	≤0.05	≤0.04	≤0.04	
Galena										
Min	≤0.04	0.27	0.18	≤0.04	≤0.04	≤0.07	84.41	≤0.07	0.09	4
Max	≤0.04	0.91	0.52	0.13	≤0.04	≤0.07	85.87	≤0.07	0.17	
Mean	≤0.04	0.53	0.38	0.07	≤0.04	≤0.07	85.04	≤0.07	0.12	
Chalcopyrite										
Min	0.06	30.18	24.59	0.41	≤0.03	≤0.04	≤0.04	≤0.04	≤0.04	3
Max	0.12	36.67	34.33	1.42	0.06	≤0.04	≤0.04	≤0.04	≤0.04	
Mean	0.08	34.32	28.33	0.83	0.05	≤0.04	≤0.04	≤0.04	≤0.04	
Bornite	0.12	14.32	58.05	0.15	0.07	≤0.04	≤0.04	≤0.04	≤0.04	1

[a] *n*: number of microprobe analyses

tion V produces etching pits on ZnS after 5–15 min; the other two solutions act much more slowly. The progress of etching (dissolution) depends strongly on the iron content of the sphalerite. Iron-rich ZnS soon becomes coated with a passive iron oxide film which slows down or even completely stops visible etching.

Metallic copper

Metallic copper occurs as minute inclusions in the silicate matrix together with metallic iron. It forms grains up to 10 μm in size. It may contain up to 2 weight percent of Ag. It is a rare phase.

Chalcopyrite group

Minerals of composition close to that of chalcopyrite, $CuFeS_2$, form common inclusions in the silicate matrix. These minerals are often intergrown with sphalerite either forming larger grains or lamellae in sphalerite where submicroscopic inclusions of $CuFeS_2$ raise the Cu content to 1.78 weight percent (Table 3). The chalcopyrite studied contains up to 1.42 weight percent of Zn (Table 3).

Bornite (Cu_5FeS_4)

A first variety of bornite is present in a characteristic textural form. In almost all the observed cases it forms a myrmekitic intergrowth with galena. Such tight intergrowths of two so different minerals suggest that myrmekitic microtextures have been produced by exsolution from the MSS (monosulfide solid solution) during cooling of the slag material. The bornite studied is characterized by a significant Fe excess (Table 3). A similar Fe excess is observed in some naturally occurring bornites.

A second variety of bornite grains, up to 0.2 mm in size, occurs separately from galena. They show various stages of replacement by covellite. The iron content is more than would be expected for Cu_5FeS_4.

Solid solution series (MnS–ZnS–FeS, alabandite)

In the samples studied, isotropic sulfides with optical properties similar to those of alabandite are present. They have a higher reflectance in air (ca. 25%) than sphalerite. The grain size of this mineral varies from a few to 30 μm, and the mineral is present as abundant inclusions in Ca–Al silicates and in corundum.

Four microprobe analyses of the mineral gave an intermediate composition between the MnS–FeS–ZnS end members. Two of the grains analyzed are Zn-rich with a Zn concentration higher than Mn + Fe, one grain has more Fe than Mn + Zn, and one grain has higher Mn + Fe than Zn content (Table 3). The MnS–FeS solid solution series is continuous up to 68.85 weight percent of FeS (Skinner and Luce 1971). The Zn alabandite has a cubic unit cell with $a = 5.204 \pm 0.009$ Å.

Metallic lead

Metallic lead is a common phase in the samples studied. It forms grains up to 5 mm in size and is directly intergrown with FeAs, ZnS, PbS, pyrrhotite, rarely marcasite, secondary anglesite, and Fe_2SiO_4 (Fig. 6). It has characteristic optical properties in reflected light, including bad polishing properties. Metallic lead contains up to 4.29 weight percent Sb (Table 1). Traces of S, Fe, and Cu are also observed.

On immersion in solutions I and II, metallic lead becomes coated with a dark oxide film within 20 min and 5 min, respectively. After this time no further progress of etching was observed under the microscope over the test periods. No etching was noted when solutions III, IV, and V were applied to the polished sections containing metallic lead. However, metallic lead dissolves in solutions VI and VII within a few minutes.

Galena (PbS)

PbS is an important component of sulfide parageneses. PbS forms intergrowths with metallic Pb and with bornite and typically may be intergrown with ZnS and with pyrrhotite (Fig. 7). The PbS studied contains significant admixtures of Fe (0.27–0.91 weight percent), Cu (0.18–0.52 weight percent), and Sb (0.09–0.17 weight percent) (Table 3).

During leaching tests on polished sections, slight etching occurs in solution I after 15 min and in solution II after 4 min. Polishing scratches are marked by a black precipitate. The same happens at contact lines between PbS and pyrrhotite. After 30 min in solution I and 8 min in the

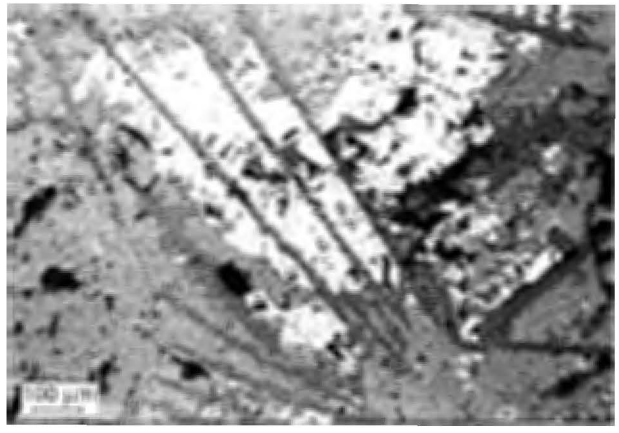

Fig. 7 Microphotograph of typical, complex mineral intergrowth of galena (white), galena–bornite myrmekite, pyrrhotite (light grey), sphalerite (grey), spinels (grey, isometric), and apatite laths (grey) set in the fayalite matrix. Reflected light, sample 23/A, scale bar 100 μm

solution II, a quarter of the galena surface is covered with a black coating. Etching pits are observed at galena–pyrrhotite boundaries after 40 and 30 min, respectively. During further etching, the thickness of the black coating on galena increases and subsequently slows down the further progress of etching. Energy dispersive spectra (EDS) on the SEM indicate that the black coating consists of lead sulfate and probably oxide as well. Galena is etched by solutions III, IV, and V in a similar manner to that described above, the progress of etching being slowed down by thickening of the coating of insoluble lead sulfate. Solutions VI and VII are good solvents for PbS.

Metallic iron (α-iron)

Metallic iron forms common oval inclusions in fayalite, iron–melilite matrices, and corundum. The grain size varies from a few up to 5 mm. Metallic iron forms intergrowths with metallic lead and pyrrhotite or is present as individual grains in the fayalite matrix. Microprobe analyses indicate that metallic Fe is strongly enriched in As but also contains significant amounts of Sb and Cu (Table 1).

Cohenite (Fe_3C)

Cohenite (Fe_3C) is mostly a constituent of rounded inclusions in the silicate matrix. It is present either as individual grains or in the form of rounded bodies composed of Fe_3C, Fe_3P, and pyrrhotite. The size of cohenite grains varies from a few to 60 μm. Some of the grains have a pronounced cubic shape.

The chemical composition of the studied Fe_3C is close to the ideal formula. Some of the grains measured may contain up to 1 weight percent of Si, so there may be some silicide admixture in some of the cohenite grains. The As content in Fe_3C is usually high (Table 4). Cu also may be present in significant amounts. The omnipresent high admixture of As may be significant from an environmental point of view. Metallic Fe and Fe_3C are unstable in the weathering zone and release soluble As complexes during decomposition.

Schreibersite (Fe_3P)

Fe_3P occurs as inclusions in silicate matrices. It forms either isolated grains or is intergrown with Fe_3C and $Fe_{1-x}S$. In reflected light it is lighter than cohenite. In oil it has a distinct pinkish brown tint that allows easy differentiation from cohenite or metallic iron. Anisotropy in air is weak but becomes distinct in oil.

The studied schreibersite has a chemical formula close to Fe_3P. It contains significant admixtures of Cu, Zn, and As (Table 4). Traces of Sb and S are also present (Table 4). Fe_3P is a potential source of As released during weathering of slag material.

Pyrrhotite ($Fe_{1-x}S$)

Pyrrhotite is a common constituent of inclusions in the silicate matrix. It is found intergrown with PbS, ZnS, Cu_5FeS_4, spinels, magnetite, and apatite (Fig. 7). It appears together with Fe, with Fe_3C and Fe_3P, and with α-(Mn,Zn,Fe)S. In the samples studied practically all of the known compositional and crystallographic forms of pyrrhotite occur, depending on mineral assemblage buffering this iron sulfide.

The $Fe_{1-x}S$ studied shows a substantial admixture of Cu, Pb, Sb, and As (Table 3). Since pyrrhotite is a common mineral in this slag material, its decomposition during weathering releases large amounts of poisonous Pb and As.

After immersing pyrrhotite in solution II for about 40 min, it becomes brass yellow and after another 30 min yellowish brown. No further changes were observed with solution II over a test period of 18 h. It seems that in the slightly oxidizing solution II, pyrrhotite is soon coated with a passive oxide film that prevents further leaching. Similar phenomena occur when solutions III, IV, and V are applied to the pyrrhotite.

FeAs

FeAs forms intergrowths with metallic lead (Fig. 6). The grain size may reach 60 μm. Microprobe measurements

Table 4 Microprobe composition of Fe_3C, Fe_3P, and FeAs (wt %)[a]

Mineral	Ni	Bi	P	S	Mn	Fe	Cu	Zn	As	Sb	Pb	*n*
Fe_3C[b]												
Min			≤0.04	≤0.03	≤0.01	92.40	0.10	0.08	0.06	≤0.04	≤0.04	3
Max			1.03	≤0.03	0.08	94.56	2.06	1.56	0.95	0.41	0.10	
Mean			0.37	≤0.03	0.06	93.56	1.08	0.68	0.63	0.16	0.18	
Fe_3P												
Min			15.81	0.23	≤0.01	80.61	≤0.03	≤0.03	0.21	0.05	≤0.04	3
Max			16.30	0.30	0.03	81.24	1.27	1.29	0.66	0.13	0.07	
Mean			16.11	0.27	0.02	80.94	0.45	0.80	0.46	0.08	0.05	
(Fe,Ni)As												
Min	5.26	0.50		0.41	≤0.03	34.21	0.08	≤0.02	54.11	0.90	0.30	3
Max	8.11	0.97		0.58	≤0.03	36.11	0.16	≤0.02	55.04	1.12	0.48	
Mean	7.02	0.80		0.52	≤0.03	34.49	0.13	≤0.02	54.51	1.01	0.36	

[a] Sought but not detected: Ag ≤ 0.04, Cd ≤ 0.03. *n*: number of microprobe analyses
[b] Contains also ~4–5 wt % C (by difference)

Table 5 Microprobe composition of Fe–Mg silicates (fayalite) (wt %)[a]

	Na_2O	MgO	Al_2O_3	SiO_2	P_2O_5	K_2O	CaO	TiO_2	V_2O_3	MnO	FeO	ZnO	*n*
Min	0.04	0.30	0.07	25.57	≤0.03	≤0.02	0.17	≤0.03	≤0.03	1.89	55.70	1.12	5
Max	0.12	4.86	0.17	30.31	2.40	0.52	2.28	0.06	0.20	3.15	63.74	6.11	
Mean	0.08	2.27	0.40	28.56	0.81	0.13	1.35	0.04	0.32	2.44	59.68	3.43	

[a] Sought but not detected: $Cr_2O_3 \leq 0.01$. *n*: number of microprobe analyses

indicate a composition of (Fe,Ni)As with significant amounts of S and Sb (Table 4). The mineral also contains up to 0.48 weight percent of Pb and some Bi (Table 4). The FeAs studied is common enough to control the As budget of the silicate slag.

Mg-Fe silicate (olivine)

$(Fe,Mg)_2SiO_4$ is one of the major components of silicates. It appears together with all of the primary phases: phosphides, carbides, sulfides, metallic iron, metallic lead, and coal residues. It forms complicated intergrowths with melilite (Fig. 5) and sulfides, mainly wurtzite, as well as with spinels, and apatite (Fig. 7).

The Fe olivine studied (Table 5) shows a low admixture of Al_2O_3, P_2O_5, and CaO. The MnO content is significant and Zn, which appears to be one of the major cations, seems to be substituted for Mg as the two elements appear antipathetic (Table 5). The solid-solution series Fe_2SiO_4 (fayalite, orthorhombic)—Zn_2SiO_4 (willemite, trigonal) is only continuous up to 17 mol percent of Zn_2SiO_4 (13.37 weight percent of ZnO) from the fayalite end member (Ericsson and Filippidis 1986). Therefore, the observed 6.11 weight percent of ZnO (Table 5) may be easily accepted by the fayalite lattice. The olivine studied is close to the Fe_2SiO_4 end member (Table 5).

Leaching tests performed on the polished specimens indicate that the olivine studied (fayalite) is resistant to solution I, as no dissolution was observed after 30 min. Solution II (pH 2) showed incipient etching of fayalite after 5 min, but this is discernible only at the crystal boundaries. After 11 min the contacts between the host fayalite and enclosed spinels became more visible. After 20 min, etching slowly developed along polishing scratches. After 6 h, all the contacts between fayalite crystals were distinctly etched, and faster etching of some crystal, depending on crystallographic orientation with respect to the polished surface, became apparent. After 18 h, the fayalite surface was covered by a thin variegated coating of Fe hydroxides, which slows down further dissolution on thickening. This coating also contains some silica as shown by EDS survey.

Solutions III and IV show weak etching of the olivine studied. It is more resistant to dissolution than are sulfides and melilite (Table 6). Its response to solution V is similar, although the first visible effects of etching appear earlier, after about 30 min. The progress of etching is slow and is

Table 6 Etching properties of solutions II, III, IV, V, VI, and VII, applied to polished surfaces of selected samples

Sample	Main minerals	Leaching medium	Leaching order
PL-D8	ZnS, PbS, FeS spinels native Pb apatite	II	apatite > galena > sphalerite ≫ pyrrhotite, wurtzite > melilite ≫ fayalite
		III, IV	galena > sphalerite > pyrrhotite, wurtzite > apatite > melilite ≫ Fe spinel > fayalite (very weak etching)
		V	galena > sphalerite > apatite ≫ pyrrhotite, wurtzite > melilite > fayalite ≫ Fe spinel > Al spinel
PL-A1	coal/anthracite/graphite goethite/limonite matrix: fayalite + inclusions of Fe_3P, Fe_3C, α-Fe	III, IV	$Fe_3P > Fe_3C >$ limonite > α-Fe (others are not affected over tested period)
		V	$Fe_3P > Fe_3C >$ limonite ≫ α-Fe > sphalerite > pyrrhotite, wurtzite > melilite ≫ fayalite
PL-X2	zincite, hydrozincite limonite azurite graphite clay-minerals	III, IV, V	hydrozincite > zincite > azurite > > > limonite
PL-23	Pb, PbS, ZnS, FeS_2, bornite matrix: fayalite	VI, VII	Pb > galena (sphalerite, bornite, melilite, fayalite are not affected)

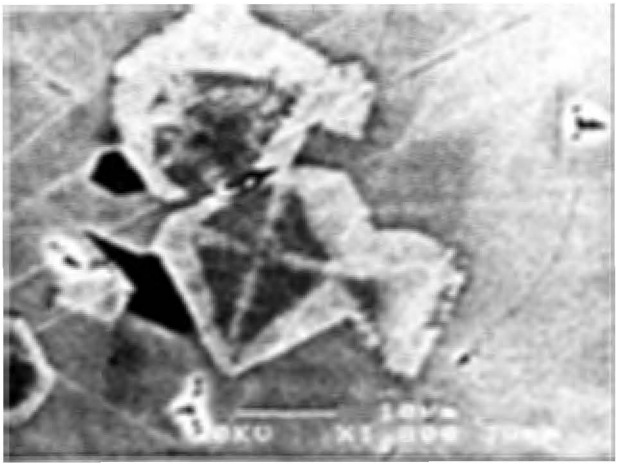

Fig. 8 SEM photograph of spinel. The interior darker part is composed of Al–Cr–V spinel while external brighter rim is made of Fe–Al spinel. The matrix is composed of melilite. Sample 23/D

kept slow by subsequent coating with a silica film, as indicated by SEM.

Spinels

Spinels of various composition, size, and optical properties are very common minerals intergrown with sulfides, apatite, and Fe olivine (Fig. 7). Those studied are zoned (Fig. 8). The outermost zone appears brighter on the SEM pictures and is rich in Fe and Ti (Table 7) and close in chemical composition to Ti magnetite. The inner zone is Al-rich and appears on the SEM pictures as the darkest one (Fig. 8). The inner core is again slightly brighter and is strongly enriched in Cr and V (Table 7).

All spinels analyzed have a high Zn content, which decreases only in magnetite-type spinels. Ti and V are antipathetic and accordingly only a little V is present in magnetite (Table 7). Since they have high Fe^{2+} contents, they are metastable during weathering and will release heavy metals. The most harmful to the environment would be Cr, which even in small quantities in drinking water causes liver damage.

No etching of spinels was observed in polished surfaces with solutions I and II. Solutions III and IV cause only slight etching on Fe spinels. After a few hours of exposure to fluid V, slight etching was also observed on Al spinels. However, the etching of all spinels is extremely weak and consequently spinels are the most resistant among the minerals tested in this study.

Corundum (Al_2O_3)

Al_2O_3 forms grains up to 1 mm in size. It usually contains numerous small inclusions of dusty Fe_3C, Fe, and Fe_3P. Al_2O_3 is enclosed in the melilite matrix that may partly replace Al_2O_3. The Al_2O_3 studied contains 5.05–6.32 weight percent of PbO. The presence of Al_2O_3 has been confirmed by XRD.

Melilite

Minerals of this type $(Ca,Na)_2(Mg,Fe^{2+},Fe^{3+},Al)Si_2O_7$ are common in volcanic lava and in blast-furnace slags. They vary widely in chemical composition and accommodate in their structure a number of heavy metals such as Zn, Ba, Mn, Fe, etc. The melilite studied contains significant amounts of Zn and Ba (Table 8), and it appears intergrown with sulfides and Fe olivine (Fig. 5). It is a very common phase in the samples studied and therefore has an important bearing on the budget of heavy metals residing in the dumps.

Leaching tests performed with solution II indicate noticeable etching effects as early as 2 min. Prolonged etching shows slow progress along crystal edges and crystal

Table 7 Microprobe composition of spinels (wt %)[a]

	Na_2O	MgO	Al_2O_3	SiO_2	CaO	TiO_2	V_2O_3	Cr_2O_3	MnO	FeO	Fe_2O_3	ZnO	*n*
Min	≤0.03	≤0.02	6.48	0.21	≤0.04	0.33	≤0.05	≤0.03	0.47	10.16	10.28	3.37	10
Max	0.34	1.79	44.39	0.97	0.13	7.17	3.81	8.88	0.72	28.35	53.68	18.48	
Mean	0.13	0.55	25.31	0.59	0.08	3.49	1.10	0.97	0.55	21.82	33.85	12.15	

[a] Sought but not detected: $K_2O \leq 0.02$. *n*: number of microprobe analyses

Table 8 Microprobe composition of Ca–Fe aluminum silicates (melilite) (wt %)[a]

	Na_2O	MgO	Al_2O_3	SiO_2	P_2O_5	K_2O	CaO	TiO_2	V_2O_3	MnO	FeO	ZnO	BaO	PbO	*n*
Min	0.04	≤0.03	10.43	0.24	≤0.03	≤0.03	0.34	0.05	≤0.03	≤0.03	1.40	≤0.05	≤0.07	≤0.03	5
Max	0.53	3.65	91.27	66.92	≤0.03	1.88	17.68	0.85	≤0.03	1.94	17.59	7.08	5.34	6.32	
Mean	0.31	0.82	41.49	30.00	≤0.03	0.83	0.36	0.38	≤0.03	0.66	8.43	3.47	2.16	2.29	

[a] Sought but not detected: $Cr_2O_3 \leq 0.01$. *n*: number of microprobe analyses

boundaries between melilite and inclusions of sulfide and spinel. The progress of melilite dissolution depends on the orientation of the crystal grains with respect to the polished surface. The difference in dissolution rate is visible after 11 min. All melilite visible on the polished section was dissolved after 170 min in solution II.

Melilite starts to show microscopically visible etching after 60, 50, and 30 min in solutions III, IV, and V, respectively. Prolonged immersion in these fluids causes slow but steady progress in etching, which is most advanced for fluid V with the lowest pH.

Apatite [$Ca_5(F,Cl,OH)(PO_4)_3$]

Apatite is a common mineral in samples with relatively high copper and lead contents. It occurs as crystals, up to 1 cm long, with long prismatic habit usually terminated by a prominent pyramid of the first order. Apatite is usually intergrown with a sulfide assemblage composed of galena, bornite, pyrrhotite, and spinels (Fig. 7). The main admixtures in the calcium phosphate studied are (weight percent): Fe 0.64–2.73, K 0.33–0.54, Zn 0.30–0.56, Si 0.11–0.35 and Pb $\leq$0.09–0.43. Some chlorine was also detected in EDS spectra of the SEM.

Leaching tests performed with deionized water at pH 5 (solution I) indicate that microscopically visible dissolution occurred within 9–12 min. With a pH 2 (solution II) dissolution was faster and visible effects occurred within 1 to 3 min; after 8 min apatite was deeply etched, leaving behind deep voids. After 110 min all microscopically visible apatite had been dissolved.

In solutions III and IV, apatite was etched after the sulfides but before melilite and fayalite (Table 6). In fluid V, apatite was etched after sphalerite but before pyrrhotite and wurtzite (Table 11). This test suggests that natural fluids residing in the dumps with pH 6.8–8.0 (fluid III) will dissolve heavy metal sulfides before apatite; this may prevent precipitation of insoluble phosphates of heavy metals in the dumps, and as a consequence these metals will be leached away.

Mineralogy and geochemistry of coal-rich black material

Coal- and graphite-rich material, important constituents of the dump material at Plombières, formed in the smelting furnace because of incomplete combustion. It contains (weight percent): Fe 5.64–13.2, Mn 0.15–0.37, Zn 1.16–4.31, Pb 2.26–3.70, and (ppm): Cd 13.0–57.0 and Cu 252–1250. Unlike silicate slag, it is rich in Cd and almost twice as rich in Pb. The fragments of carbonaceous matter reach a few centimeters in size. The material is intermixed and intergrown with minor slag products such as silicates containing inclusions of metals and sulfides described in the section devoted to slag material. However, as indicated by microprobe analysis, most of the lead is directly bound to carbonaceous matter (Table 9) and is therefore not bound to fragments of silicate slag material.

Anthracite–graphite–coal

Anthracite-graphite is a very common primary constituent of coal-rich black material. The reflectivity of the carbonaceous material varies from that of high vitrinite to that of graphite proper, showing all intermediate gradations. All the carbonaceous fragments are very anisotropic in reflected light. Some of the anthracite–graphite forms tight intergrowths with iron oxides and silicates. Some of the anthracite grains have well-preserved microstructures of coal (organic structures).

Coal–anthracite–graphite grains are rich in several heavy metals (Table 9). The most significant are Fe and Pb, but no visible inclusions of iron or lead minerals have been observed, either in reflected light microsopy or during SEM check. This suggests that Fe and Pb may be organically bound, so that Pb would be released to the ground waters by slow oxidation of organic matter present in the dumps.

No etching of the graphite–coal surface by the leaching fluids was observed over a test period of 18 h.

Mineralogy and geochemistry of clay from mineral dressing waste

Yellow to yellow–brown clay material appears in the dumps associated with fine-grained dolomite sand. It contains on average (weight percent): Fe 11.9, Mn 0.04, Zn 0.82, Pb 2.15, and (ppm): Cd 27 and Cu 94. The main mineral is illite with a small but significant admixture of kaolinite. The latter, however, does not constitute more than 10–20% of the clay fraction. A high admixture of Pb in this material of mineral dressing waste is probably connected with the poor benefication technology. Galena is

Table 9 Microprobe composition of coal–anthracite–graphite grains (wt %)[a]

	Mg	Al	Si	P	S	Mn	Fe	Ni	Cu	Zn	As	Pb	*n*
Min	$\leq$0.01	0.06	0.34	$\leq$0.02	0.26	0.26	0.59	$\leq$0.01	$\leq$0.01	0.19	$\leq$0.01	0.15	4
Max	0.08	0.33	0.61	0.30	0.61	0.58	18.66	0.29	0.11	1.25	0.05	5.73	
Mean	0.05	0.18	0.48	0.10	0.46	0.38	8.09	0.09	0.04	0.83	0.03	3.88	

[a] Sought but not detected: Ag $\leq$ 0.02, Cd $\leq$ 0.02, Sb $\leq$ 0.02. *n*: number of microprobe analyses

very brittle and is often milled to a size too small for recovery by flotation or gravity methods. In this way galena is rejected with the mineral dressing wastes even in modern mineral processing plants.

Mineralogy and geochemistry of mining wastes

The main components of mining wastes are carbonate host rock and iron oxides, which are common constituents of weathered Zn–Pb ores. Occasionally, fist-size specimens of massive galena, pyrite–marcasite, and banded sphalerite were found in this waste type. The metal budget of mine wastes is controlled by iron oxides, which are a major mineral constituent. The amount of anglesite is also significant. Zn siderite and Fe smithsonite are less abundant. Most of the primary pyrite–melnikovite has probably been already converted into iron oxides. The primary iron oxides found in mine wastes may be a significant source of poisonous As and Tl (Table 10).

Iron oxides

The iron oxides at Plombières mainly consist of goethite and amorphous iron oxide with traces of lepidocrocite. Naturally occurring iron oxides in the Zn–Pb mines of Plombières were strongly enriched in Zn, S, and Pb (Table 10) and also contained a high admixture of As and up to 0.46 weight percent of Tl. In iron oxide containing the highest content of As, beudantite [$PbFe_3(AsO_4)(SO_4)(OH)_6$] has been identified by reflected light microscopy and confirmed by microprobe and x-ray diffraction. Beudantite explains a significant portion of Pb and As residing together with S in iron oxides. The remaining Pb is probably present as microinclusions of anglesite and lead oxides. Thallium is present in iron oxides enriched in sulfur.

Anglesite ($PbSO_4$)

Anglesite is the second most common mineral associated with weathered Zn–Pb ores in the Plombières dumps. It contains significant admixtures of Si and traces of Zn (Table 10). The mineral usually forms boxwork textures.

Zn siderite and Fe smithsonite

Zn siderite and Fe smithsonite are found as inclusions in iron oxides or as a component of boxwork textures together with anglesite. In the samples studied they do not form a continuous series (Table 10).

Pyrite and melnikovite

Pyrite and melnikovite are common constituents of the sulfide ores exploited in Belgium. Melnikovite was re-

Table 10 Microprobe composition of iron oxides, sphalerite, pyrite, melnikovite, anglesite, Zn siderite, and Fe smithsonite found in mine waste (wt %)

Mineral	Al	Si	S	Fe	Ni	Zn	As	Tl	Pb	n^a
Iron oxides										
Min	≤0.03	0.04	0.44	4.29	≤0.04	0.12	≤0.05	≤0.04	0.18	50
Max	6.21	5.43	15.58	49.28	1.71	24.75	17.64	0.46	10.89	
Mean	0.26	1.16	3.31	33.24	0.07	4.35	2.47	0.07	2.34	
Sphalerite[b]										
Min	≤0.04	≤0.03	25.81	0.15	≤0.05	48.10	≤0.05	≤0.06	≤0.05	40
Max	≤0.04	0.36	32.11	15.18	3.69	65.45	1.00	0.18	0.68	
Mean	≤0.04	0.16	29.20	6.82	0.24	60.07	0.28	0.09	0.24	
Pyrite										
Min	≤0.03	≤0.01	39.98	14.09	0.03	0.13	0.09	≤0.04	1.29	17
Max	≤0.03	0.36	51.81	45.20	9.09	28.36	3.54	0.24	11.19	
Mean	≤0.03	0.08	46.22	32.97	4.38	4.97	2.46	0.07	6.11	
Melnikovite										
Min	≤0.03	≤0.03	2.76	0.35	0.07	≤0.04	0.15	≤0.05	≤0.05	22
Max	0.30	1.51	49.22	48.99	0.32	29.86	7.92	2.29	75.70	
Mean	0.07	0.39	22.74	25.19	0.19	2.38	2.85	0.50	18.07	
Siderite										
Min	≤0.03	≤0.03	≤0.03	41.18	≤0.03	1.53	≤0.05	≤0.04	≤0.07	15
Max	≤0.03	0.21	≤0.03	46.40	≤0.03	6.84	≤0.05	≤0.04	≤0.07	
Mean	≤0.03	≤0.03	≤0.03	43.21	≤0.03	4.91	≤0.05	≤0.04	≤0.07	
Smithsonite										
Min	≤0.03	≤0.03	≤0.04	8.80	≤0.04	40.11	≤0.05	≤0.05	0.38	5
Max	0.04	≤0.03	≤0.04	9.23	≤0.04	41.10	≤0.05	≤0.05	0.64	
Mean	≤0.03	≤0.03	≤0.04	9.12	≤0.04	41.03	≤0.05	≤0.05	0.42	
Anglesite										
Min	≤0.05	0.05	10.15	0.22	≤0.05	≤0.07	≤0.07	≤0.07	67.62	5
Max	≤0.05	1.28	10.82	0.26	≤0.05	0.40	≤0.07	≤0.07	67.80	
Mean	≤0.05	0.62	10.48	0.24	≤0.05	0.18	≤0.07	≤0.07	67.68	

[a] *n*: number of microprobe analyses
[b] Contains also 0.28–1.60 wt % of Cd

cently redefined (Kucha and Viaene 1993) as a compound composed of metals with sulfur of mixed and/or intermediate valences. Pyrite and melnikovite are both rich in As and Pb and may contain high contents of poisonous Tl (Table 10).

Summary of leaching tests

Solution I (pH 5) affected only some of the minerals. It dissolved metallic zinc but not its alloys. After 20 min of etching, the surface of metallic lead was coated with a black precipitate that prevented further dissolution. Galena was coated with a similar black precipitate after a few hours of etching. Solution I also slowly dissolved iron carbides and phosphides. Other minerals were not reactive to solution I over test periods of 18 h.

Leaching medium II (pH 2) etched the same minerals affected by fluid I, but faster. It also dissolved ZnS slightly along crystal boundaries and polishing scratches. Solution II etched pyrrhotite and subsequently covers its surface after 40 min with a brownish passive film that stops further etching. Unlike solution I, solution II etched fayalite. At first it etched only crystal boundaries (6 h), but after 18 h it coated the surface with a passive oxide film stopping further etching. Solution II also etched melilite and apatite.

The etching tests using solutions I and II show that these acid fluids will mobilize metals that form soluble oxides/hydroxides or sulfates (Zn, Cd), while those forming insoluble or weakly soluble salts (Fe, Pb) will remain within the dump.

The pH differences between solutions III (pH 7.5), IV (pH 5), and V (pH 4) give rise to a different etching order of minerals (Table 6, sample PL-D8). Only the more soluble minerals were affected by the less acid solutions III and IV (Table 6, sample PL-A1). In general, solutions III, IV, and V with a composition similar to the pore waters of the dumps eventually dissolve silicates and release bound heavy metals. Leaching by pore waters is strongly pH dependent and may be controlled by the availability of sulfides in the dump material, because this mineral, upon oxidation, creates a strongly acidic environment (Neumann-Mahlkan 1993). Microbial leaching may be an additional control. However, this process has not been investigated.

The higher solubility of metallic lead than that of galena in solutions VI and VII calls for a careful interpretation of sequential leaching tests, where sodium acetate solutions are used to measure exchangeable cations (pH 7) or to determine the carbonate content (pH 5). During such tests performed on our samples, most of the lead in solution came from dissolved metallic lead. This was confirmed by leaching tests performed on the surfaces of polished sections containing metallic lead. Only very weak etching was observed on the surface of cerussite ($PbCO_3$).

Discussion

Almost all of the primary phases discussed are metastable at surface conditions. The most vulnerable ones are those containing sulfidic sulfur and/or divalent iron. Sulfides decompose mainly by sulfur oxidation. In this process sulfur forms a very soluble sulfate, which transports all of the metals except Fe^{3+} and Pb because $PbSO_4$ has a low solubility at the pH prevailing within the pore network of the dump, where it is buffered by carbonates. It is to be expected that Zn and Cd will be mobilized in this way.

The Plombières and La Calamine dumps are located directly on the banks of the Geul river valley and have been a source of significant downstream heavy-metal pollution (Leenaers 1989; Swennen and others 1994). Small-scale mining occurred in the area as early as the Middle Ages (Dejonghe and Jans 1983). Industrial mining and smelting took place at La Calamine between 1806 and 1882, at Plombières between 1844 and 1882, and at Schmalgraf between 1868 and 1932. The mining and smelting activities in the area stopped around 1936. The first ore body consisted of oxidic Zn ore, the two others were composed of Zn, Pb, and Fe sulfides (Dejonghe and Jans 1983; Dimanche and others 1979; Ladeuze and others 1991). The type of contamination of the Geul river overbank sediments depends strongly on the nature and time of the mining activity upstream (Swennen and others 1994). The earliest mined ore of La Calamine consisted of oxides, and the beginning of its exploitation in 1806 correlates with a sudden increase of Zn and Cd in the Geul sediments (Swennen and others 1994). The onset of the Zn–Pb–Fe sulfide ore mining in 1844 is marked in the overbank sediments by an abrupt increase of Pb and Cu, while Cd retains its high concentration. This pattern is consistent with major and trace elements present in the exploited oxide and sulfide ores. After 1882, the Pb, Cd, and Cu contents in the Geul sediments decrease parallel with decreasing industrial mining in the area. However, the Zn content in these sediments remained unaffected by the intensity of mining after this date and stayed at a high level (Swennen and others 1994). The contrasting behavior of Pb, Cu, and Cd on the one hand and Zn on the other hand is a result of the mineralogy and metal mobilities in the dumps.

Zinc in the dumps occurs mainly as substitutions in Fe–Mg and Ca–Fe silicates (Tables 5, 8), Cd-free sulfides (Table 3), and less so as oxides containing some Cd (Table 2). Leaching tests performed on polished sections indicate that sulfate–chloride fluids present in the pore networks of the dumps will leach Zn from all the main mineral phases, providing a steady supply of this metal into the Geul river in the form of soluble sulfates and chlorides. The process is likely to continue until all available zinc is leached away. Only a minor part of the Zn is trapped within the dumps as substitutions in less soluble or insoluble secondary phosphates.

Cadmium was present in the oxide ore of La Calamine and occurred in the sulfide ore of Plombières, where it

potentially replaced zinc in sphalerite. Thus, a high Cd content is observed in the river sediments (Swennen and others 1994) regardless of the type of ore that has been mined. In the Plombières dumps Cd is present in zinc oxide of the slag material (Table 2), as well as in sphalerite in the mine waste (Table 10). Both forms are soluble in dump fluids and will discharge Cd together with Zn into the Geul river. However, the principal zinc carriers in slag —silicates and sulfides—have very low Cd contents, so that a high rate of Zn discharge will be coupled with a smaller Cd output.

Lead has a low mobility in the leaching fluids tested except in those with sodium acetate. Both metallic lead and galena are covered with low solubility products that retard the process of dissolution. Some lead is trapped in the dumps as insoluble sulfates and phosphates. However, sodium acetate is a very good solvent for lead, and some natural analogs of this compound may greatly increase the mobility of Pb. The observed low solubility of lead may mean that it is dispersed downstream as fine particulate matter. Otherwise, we have no explanation for the high concentration of Pb in downstream sediments (Swennen and others 1994) in view of the relatively alkaline pore networks of the dump caused by a high carbonate content. Under such conditions Pb should not be leached (Sangameshwar and Barnes 1983).

Arsenic is present as iron arsenide in slags (Table 4) and as melnikovite in mine wastes (Table 10). Both compounds are unstable and will release mobile arsenates upon weathering. Indeed, arsenic contamination is observed in river sediments (Swennen and others 1994).

Thallium is present in the dumps in ZnO (Table 2) of slag material and in iron oxides and melnikovite of the mine waste (Table 10). The observed amounts of Tl are dangerous in view of its high toxicity. Tl is very mobile in most natural environments as Tl^+ and disperses easily during oxidation of thallium-bearing sulfides (Vink 1993). No systematic measurements of the Tl abundances in the Plombières dumps and in downstream sediments have been made. However, given the toxicity of Tl and its presence in some of the dump minerals, such a study should be undertaken.

Phosphorus seems to play a special mitigating role in metal mobilities. It occurs in slags as iron phosphides (Table 5) and apatite. During weathering, the released phosphate reacts with Fe, Pb, Cu, and Zn, forming low-solubility products coating slag aggregates. Thus P plays a significant role in the retardation of heavy metal discharge from the dumps by forming protective surface coatings and low-solubility reaction products with heavy metals. However, the amount of P occurring in the slags is insufficient to block metal leaching. The significant and positive role of phosphates in remediation of contaminated land has been confirmed by a practical application (Cotter-Howells and others 1994). Application of phosphate armor seems to be the fastest and cheapest way to block dispersion of heavy metals by the formation of insoluble phosphates (Blowes and others 1994). The ubiquitous natural formation of heavy-metal phosphates in the Plombières dumps from phosphorus in the form of phosphides and apatite in slags leads us to propose the application of phosphate in order to stabilize the chemical load of the dumps. The influence of such addition can be tested at the dump site for a year and could provide an estimation of phosphate trapping efficiency. A suitable experiment can be easily designed and carried out at a relatively low cost.

Buffering by carbonates present in the mine wastes piled up at the Plombières dumps also retards the metal discharge from the dumps. The carbonates keep the pH of the pore fluids typically between 6.8 and 8.0. In this pH range weathering of the dump material produces much gypsum, lead sulfates, and phosphates, all of which slow down the leaching of this metal.

The Plombières wastes were randomly deposited during the period 1806–1932, at a time when no attention was paid to environmental considerations. At this site, the period of most intense sulfide oxidation and the associated release of dissolved metals has now passed. However, judging from the metal amounts and their mineralogical forms, the transport of oxidation products of sulfides and silicates through the waste pile will continue at least for several decades. Several remedial procedures have recently proved useful for the reduction of the impact of mine wastes on the environment (Blowes and others 1994). Some of these procedures can be considered for the Plombières site:

1. Installation of sulfate-reducing porous reactive walls in the path of fluids leaving from the dumps. This technique is usually recommended for older tailings in which the peak period of sulfide oxidation has passed. However, the Plombières dumps contain smelting slags as well as mine wastes. In these slags about half the Zn is present in the structure of iron silicate (olivine) and is released upon oxidation. Therefore the zinc outflow is expected to remain high for a few decades, which would require maintaining a water-treatment plant for this duration. The related maintenance costs would be high.

2. Reprocessing of the dump material and metal extraction from sulfides. This technique is economical during mineral dressing operations when waste sulfide (pyrite, pyrrhotite) can be separated from base-metal sulfides. In the Plombières case it is not recommended because many sulfides have already been oxidized and half the Zn is present in olivine.

3. Removal of the dump material and redeposition in an old clay pit or an artificial dump site, made impermeable by especially designed geotextiles. Precautions must be taken to monitor the discharge of metals. This is probably the best and safest solution in the long run.

4. Construction of an artificial landscape designed to create a reducing environment. This can be achieved in two ways. The first is the downstream construction of a wetland for treatment of the drainage; natural peat would fix the metals and the system would be self-sustaining, keeping maintenance costs low. The second one is the construction of a bog environment over the dump site. This solution is usually applied directly after dumping, before oxidation of the sulfides. In Plombières there is a risk that

Table 11 Microprobe composition of iron oxides (secondary) (wt %)[a]

	Al	Si	P	S	Cl	Mn	Fe	Cu	Zn	As	Ag	Pb	Mg	Ca	*n*
Min	≤0.01	0.07	≤0.03	0.05	≤0.04	≤0.01	30.87	≤0.01	≤0.03	≤0.04	≤0.04	≤0.04	≤0.01	≤0.03	11
Max	0.97	9.75	0.47	8.12	4.88	4.55	62.85	2.61	4.81	0.21	0.07	1.20	2.85	1.40	
Mean	0.19	2.20	0.13	1.77	0.52	0.49	51.65	0.32	0.87	0.06	0.04	0.21	0.30	0.45	

[a] Sought but not detected: Cd ≤ 0.04, Sb ≤ 0.04. *n*: number of microprobe analyses

during the initial period of bog construction oxidized secondary minerals containing base metals (Table 11) will be reduced and release their heavy metal load into the outflowing fluids.

5. Restriction of water infiltration into the dumps. The most effective strategy relies on restricting the entry of meteoric waters, surface water, and groundwater into the dump. The first restriction can be achieved by covering the dumps with a clay or geotextile layer. The other two would probably require the construction of an extensive dam around the site, located according to the existing groundwater circulation.

6. Sulfide and silicate oxidation controls. A clay layer on top of the dumps would restrict the entrance of gaseous oxygen. It should have a thickness of at least 2 m to prevent perforation by tree roots. A better solution would be to armor the sulfide and silicate mineral surfaces with a coating of insoluble, nonreactive precipitate, thereby isolating these minerals from oxidants (O_2, Fe^{3+}, etc.). That phosphate is the best armoring coating (Blowes and others 1994) is suggested by the abundant natural overgrowths of heavy metal phosphates from P released by oxidation of phosphides. Addition of phosphate to the dump material would probably be the cheapest and fastest local remedy (Cotter-Howells and others 1994). Sulfides in the slag form inclusions in Zn-bearing olivine. The observation of secondary phosphates indicates that they adhere tightly to the silicate surface and provide it with a firm protective armor.

Conclusions

The mineralogical analyses and the leaching tests provide a picture of the phases containing the bulk of the heavy metals and of the chemical processes responsible for dissolving and precipitating them. There is a natural geological buffer against excessive dissolution of the metals. Indeed, the carbonate rock fragments mixed in the dump material and the carbonate rocks underlying the dumps provide a neutral or slightly alkaline environment, which slows down most dissolution reactions. However, acid rain causes slow leaching of the porous dump material, and the Geul river drains the dumps directly.

Zn is the most mobile of the polluting metals and is found mainly in silicates, but also as sulfides and oxide–hydroxide.

Pb occurs mainly as metallic lead and galena, which are often coated with insoluble sulfate and phosphate, making this element relatively immobile.

Cd substitutes for Zn in both oxides and some sulfides, but the bulk of the soluble Zn minerals have a low Cd content, thus keeping the total Cd release low.

Tl and As are both mobile elements, the latter forming soluble arsenates. Minor pollutants include also Cu and Cr.

Phosphate addition seems to be the most promising of all the available techniques to shield the environment from the heavy metals in terms of cost effectiveness. Over a short period of time, soluble minerals would be coated with a film of insoluble phosphate. However, in order to justify such a procedure, a calculation of the metal content of the dumps should be carried out, based on systematic sampling, including drilling through the dumps. A feasibility study of the effect of phosphate addition on metal mobility must be tested experimentally.

Acknowledgments We thank the Geological Survey of Belgium for funding the project and for permission to publish the results. The research has benefitted from grants of the National Fund for Collective Research of Belgium for the x-ray powder diffractometer and the scanning electron microscope. The municipal authorities of Plombières are thanked for access to the dumps.

We thank R. Swennen and I. Van Keer for constructive discussion about the field relations of the dumps and G. King and the reviewer of the journal for critical reading of the manuscript. The technical assistance of D. Coetermans, H. Nijs, and D. Steeno is gratefully acknowledged.

References

Blowes DW, Ptacek CJ, and Jambor JL (1994) Remediation and prevention of low quality drainage from tailings impounds. In: Jambor JL and Blowes DW (Eds), The environmental geochemistry of sulphide mine-wastes. Waterloo, Ontario: MAC Short Course Handbook 22. pp 365–379

Brandon JK, Brizard RY, Chien PC, McMillan RK, and Pearson WB (1974) New refinements on the γ-brass structures Cu_5Zn_8, Cu_5Cd_8 and Fe_3Zn_{10}. Acta Crystallogr B30:1412–1417

Cotter-Howells J, Caporn S, and Thornton I (1994) Remediation of contaminated land by formation of heavy metal phosphates. Abstract. 3d International Symposium on Environmental Geochemistry, 12–15 September 1994, Krakow, Poland

Dejonghe L and Jans D (1983) Les gisements plombo-zincifères de l'Est de la Belgique. Chron Rech Min 470:3–24

Dimanche F, Ek C, and Frenay J (1979) Minéralisations plombo-zincifères belges. Ann Soc Geol Belg 102:417–429

Ericsson T and Filippidis A (1986) Cation ordering in the limited solid solution Fe_2SiO_4–Zn_2SiO_4. Am Mineral 71:1502–1509

Johansson A, Ljung H, and Westman S (1968) X-ray and neutron diffraction studies on γ-Ni, Zn and γ-Fe, Zn. Acta Chem Scand 22:2743–2753

Kucha H and Viaene W (1993) Compounds with mixed and intermediate sulphur valences as precursors of banded sulphides in carbonate-hosted Zn–Pb deposits in Belgium and Poland. Mineral Deposita 28:13–21

Ladeuze F, Dejonghe L, and Pauquet F (1991) Historique de l'exploitation des gisements plombo-zincifères de l'Est de la Belgique: le rôle de la "Vieille Montagne." Chron Rech Min 503:37–50

Leenaers H (1989) The dispersal of metal mining wastes in the catchment area of the River Geul (Belgium-The Netherlands). Ned Geogr Stud 102:199 pp

Neumann-Mahlkan P (1993) Acidification by pyrite weathering on mine waste stockpiles, Ruhr district, Germany. Eng Geol 34: 125–134

Ramdohr P (1969) The ore minerals and their intergrowths, 3d ed. New York: Pergamon. 1174 pp

Sangameshwar SR and Barnes HL (1983) Supergene processes in zinc–lead–silver sulphide ores in carbonates. Econ Geol 78: 1379–1397

Skinner BJ and Luce FD (1971) Solid solutions of the type (Ca,Mg,Mn,Fe)S and their use as geothermometers for enstatite chondrites. Am Mineral 56:1269–1296

Swennen R, Van Keer I, and De Vos W (1994) Heavy metal contamination in overbank sediments of the Geul river (East Belgium): Its relation to former Pb–Zn mining activities. Environ Geol 24:12–21

Van Tassel R (1979) Minéraux artificiels ou de néoformation à Plombières et Sclaigneau. Belgique. Bull Soc Belg Geol 88:273–279

Vink BW (1993) The behaviour of thallium in the (sub)surface environment in terms of Eh and pH. Chem Geol 109:119–123